Journal of Applied Electrochemistry (2023) 53:1337–1348
https://doi.org/10.1007/s10800-023-01862-7

RESEARCH ARTICLE

High-performance IN738 superalloy derived from turbine blade waste for efficient ethanol, ethylene glycol, and urea electrooxidation

Mahmoud A. Hefnawy[1] · Shymaa S. Medany[1] · Rabab M. El-Sherif[1] · Nader El-Bagoury[2] · Sahar A. Fadlallah[1]

Received: 2 December 2022 / Accepted: 29 January 2023 / Published online: 1 March 2023

Abstract

In this work, IN738 superalloy used previously in gas turbines was recycled and used as a working electrode for the electrooxidation of different fuels, namely ethylene glycol, ethanol, and urea. The electrocatalytic efficiency of the electrode was studied by cyclic voltammetry, chronoamperometry, and electrochemical impedance. Several kinetics parameters like diffusion coefficient, Tafel slope, rate constant, and activation energy were calculated. The modified electrode was characterized as received using XRD, SEM, and EDAX to elucidate the crystal structure and surface morphology before and after electrochemical oxidation. The anodic current densities of electrochemical oxidation of ethanol, ethylene glycol, and urea were 29, 17, and 12 mA.cm^{-2}, respectively, in an alkaline solution at a potential of 0.6 V (vs. Ag/AgCl). The kinetic parameters like diffusion coefficients for ethanol, ethylene glycol, and urea were found to be 1.5×10^{-6}, 1.038×10^{-6}, and 0.64×10^{-6} cm^2 s^{-1}, respectively. The charge transfer resistances were estimated for electrooxidation of different fuels by electrochemical impedance spectroscopy (EIS).

Graphical Abstract

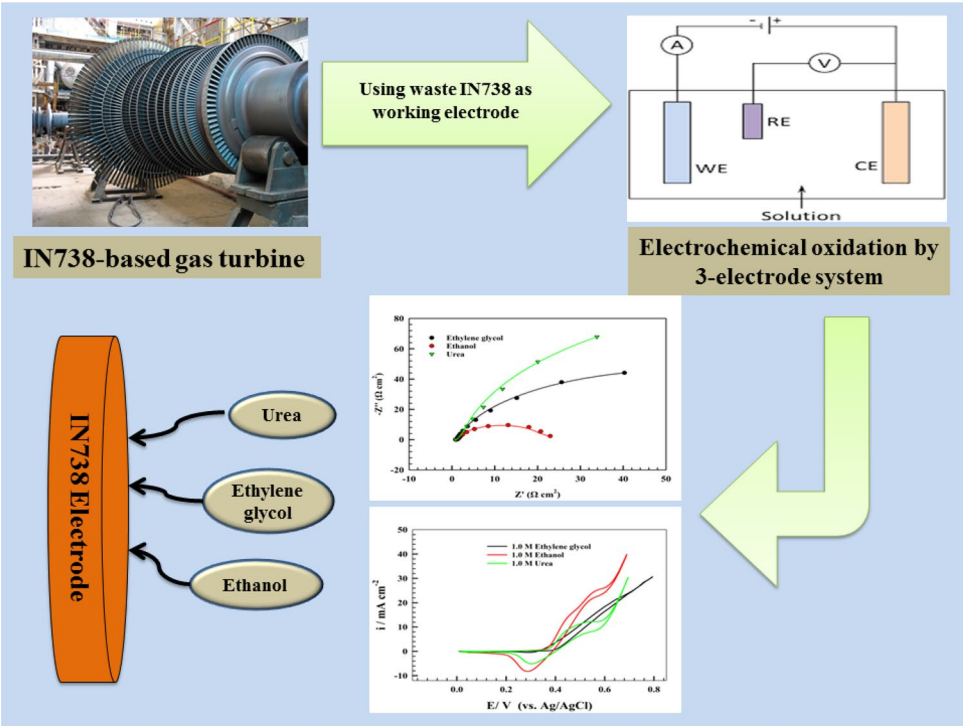

Keywords IN738 superalloy · Nickel-based superalloy · Electrocatalysis · Energy conversion · Fuel cells

Extended author information available on the last page of the article

1 Introduction

Fuel cells are a promising device that is widely used for energy generation that is clean and sustainable [1–4]. Moreover, the fuel cell is recognized as a device that generates green and sustainable electrical energy via the electrooxidation of a hydrogen-rich molecule (i.e., methanol, ethanol, formic acid, ammonia, glycerol, and urea) [5–10]. However, fuel cells have several profits over conventional combustion-based technologies used in many power plants and vehicles [11].

Fuels can be mainly classified depending on their physical state (solid, liquid, or gas), origin, and chemical structure. Several materials can be used as fuels, like ethylene glycol, ethanol, and urea [12–15]. Ethylene glycol (EG), a cheap and non-volatile material, has been interested in its lower toxicity and higher ignition point than other alcohol. Besides, the energy capacity of EG ca. 4.8 A.h.mL^{-1} is higher than methanol (4 A.h.mL^{-1}) [16]. Based on the structure of EG, the complete conversion of EG to CO_2 evaluates ten e$^-$ per one molecule of alcohol, while the reaction can be expressed as follows (Eq. (1)) [17]:

$$\left(CH_2OH\right)_2 + 2H_2O \rightleftarrows 2CO_2 + 10H + 10e^-. \quad (1)$$

Ethanol is a non-toxic liquid produced from gasoline and biomass. Ethanol is alcohol with a C–C bond that has a higher energy density compared with methanol, since it can deliver 12 electrons per molecule if fully oxidized to CO_2, as illustrated in the following Eq. (2) [18]:

$$CH_3CH_2OH + 12OH^- \rightarrow 2CO_2 + 9H_2O + 12e^-. \quad (2)$$

Urea is an impressive fuel because of its ability to be produced in large scans by the petrochemical process. In addition, urea-rich water is available in the sludge of industrial processes and human urine in the wastewater. Direct urea fuel cells (DUFCs) are one of the most rapidly growing fuel cells. Nowadays, many researchers focus their efforts on DUFC owing to a high energy density of up to 17 MJL^{-1} compared with liquid hydrogen equal to 10 MJL^{-1} [19].

The urea electrochemical oxidation is considered as six electron process which can be represented by the following Eq. (3) [20]:

$$CO\left(NH_2\right)_2 + 6OH^- \rightarrow N_2 + 5H_2O + CO_2 + 6e^-. \quad (3)$$

Several precious metals like palladium and platinum are widely used as anodic materials for electrochemical oxidations due to their high stability, low CO tolerance, and high catalytic conversion [21–25]. Recently, the nickel-based catalyst has been considered a significant element for electrochemical oxidation, compared with other precious metals, like palladium and platinum. The growing interest in Ni-based catalysts is owing to their availability, low toxicity, and cheap cost.

Consequently, modified surfaces of nickel based were reported to enhance to activity of the electrocatalyst, such as nanowire [26–28], nanofoam [29], or nanoflowers [30]. Additionally, the activity of the electrodes was reported in the literature by promoting the electronic properties using binary metals, like $NiCo_2O_4$, Ni-WO_2, Ni–Fe double hydroxides, and $LaNiO_3$, [31–34].

Turbine blades are considered the most sophisticated single-crystal superalloys globally due to the continuous material with zero grains. At the same time, the superalloy can afford extraordinary mechanical properties under elevated temperatures and high-stress conditions [35]. Ni-based superalloys are widely used for high-temperature applications, such as disks and blades of either aerospace engines or land-based gas turbines [36–39]. The gas turbine blades used for power generation are mostly nickel-based superalloys, such as IN738LC alloy. Ni-based superalloy includes several elements in crystal systems, such as tungsten, tantalum, niobium, and molybdenum [40].

The high percentage of nickel element facilitates the nickel-based superalloy suitable for electrocatalysis in an alkaline medium. On the other hand, the presence of another transition element like Cr, Mo, and Nb was proved to reinforce the catalysis potential by enhancing the electrical properties and the poisoning resistance [41–45]. Therefore, the activity of IN738 alloy is expected to be high toward the oxidation of small molecules regarding the structure and chemical composition.

In this work, IN738 electrode derived from a waste gas turbine blade was used as anode material for the electrochemical oxidation of different organic molecules, like ethylene glycol, ethanol, and urea. A comparative electrochemical study was performed, and different kinetics parameters were calculated for the different fuel oxidation upon the working electrode.

2 Experimental part

2.1 Materials, chemicals, and solvents

IN738 waste alloy was received as an old turbine blade scrap from a gas turbine power plant. The chemicals used in the electrochemical experiment were analytical grade. All solutions were prepared with double distilled water.

2.2 Catalyst synthesis

2.2.1 Preparation of IN738 superalloy

The sample was first soaked in 0.5-M nitric acid to clean the surface of any organic or carbon materials. Then, the surface

was polished with conventional sand polish paper. Finally, the electrochemical treatment was performed on IN738 sample by soaking the electrode in 1.0 M of KOH to generate the corresponding hydroxide species by cyclic voltammetry. Table 1 shows the chemical composition of the as received.

2.3 Structural and surface analysis equipment

The XRD was performed as a prepared IN738 superalloy using the Panlytical X'Pert instrument with Cu-Kα radiation (λ = 1.540Å). The Quanta 250 FEG instrument was used for scanning electron microscopy (SEM) and EDAX measurements of IN738 sample. To enhance the samples' conductivity and resolution measurement, the samples were coated with gold using EMITECH k550x sputter coater.

2.4 Electrode preparation

The electrochemical oxidation of fuel was performed on the surface of a well-polished (mirror-like) IN738 electrode (cuboid shape alloy with dimension length, width, and height ca. 5, 5, 1 mm) sealed in an epoxy resin jacket, leaving an exposed geometric surface area of 0.25 cm^2. For impurities removal, the IN738 electrode was immersed in 10% HNO_3, rinsed with distilled water, and then polished using 2500 grit emery paper to obtain a smooth mirror-finish surface. The electrochemical studies were performed using cyclic voltammograms, chronoamperometry, and the electrochemical impedance to investigate the activity of IN738 electrode toward the electrooxidation of different fuels, like ethanol, ethylene glycol (EG), and urea. The three-electrode system was used to perform the required studies in a solution containing a 1.0-M potassium hydroxide aqueous electrolyte, a platinum wire as the counter electrode, and an Ag/AgCl electrode (saturated KCl) as a reference electrode. Autolab workstation (PGSTAT128N) was employed to find the different electrochemical experiments, like cyclic voltammetry, chronoamperometry, and electrochemical impedance. Nova software (ver. 2.1) was used as a graphical user interface. The EIS experiment was measured by applying an AC Potential of 0.1 Hz up to 1×10^4 Hz. Because of the nature of the sample (metal waste), all electrochemistry results were measured three times to ensure the reproducibility of the data.

3 Results and discussion

3.1 Characterizations

3.1.1 XRD

The crystal system of the as-casted alloy was studied using an x-ray diffraction pattern. Figure 1 shows the XRD patterns of the nickel-based 738 after heat treatments. As shown in Fig. 1, the as-cast sample consists of three main phases, namely γ-Ni, γ`-Ni_3[Al, Ti], and γ``-$Ni_3$Nb, at 2Θ = 40.3, 43.9, 50.2, 74.2, 90.3, and 96.2. For phases γ-Ni and γ`-$Ni_3$[Al, Ti], the pattern is indexed to the (111), (002), (022), and (113). At the same time, the peaks for the γ``-Ni_3Nb phase are indexed to the (112), (020), (220), and (132) [46]. However, aluminum and titanium are considered essential solutes in nickel-based superalloys. Two-phase microstructure like gamma (γ) and gamma-prime (γ') is mainly responsible for the high-temperature strength and high creep deformation resistance [47].

3.1.2 Surface characterization

The morphology and elemental analysis of IN738 surface were performed by scanning electron microscope (SEM) and energy-dispersive X-rays (EDX). Figure 2a represents the SEM image of the surface of IN738 before oxidation. Due to acid polishing and surface treatment, the tunnel appeared on the alloy surface. The surface was studied after the oxidation of urea. As shown in Fig. 2b, the metal hydroxide layer

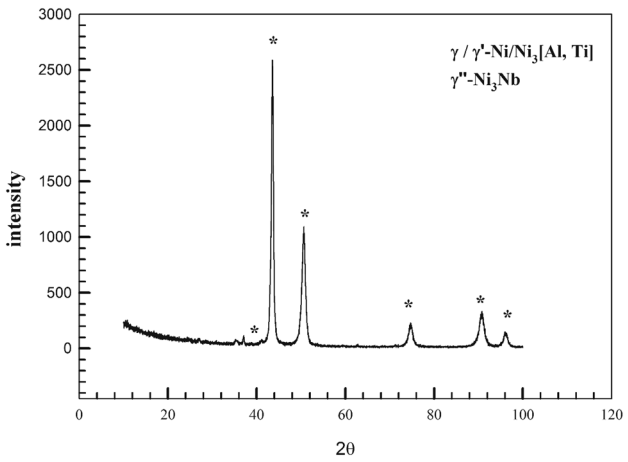

Fig. 1 XRD chart of IN738

Table 1 Elemental distribution of IN738 elements

Element	C K	O K	AlK	NbL	MoL	TiK	CrK	CoK	NiK	TaL
Weight %	11.08	4.85	3.08	0.1	0.37	3.16	13.59	6.32	51.85	3.21

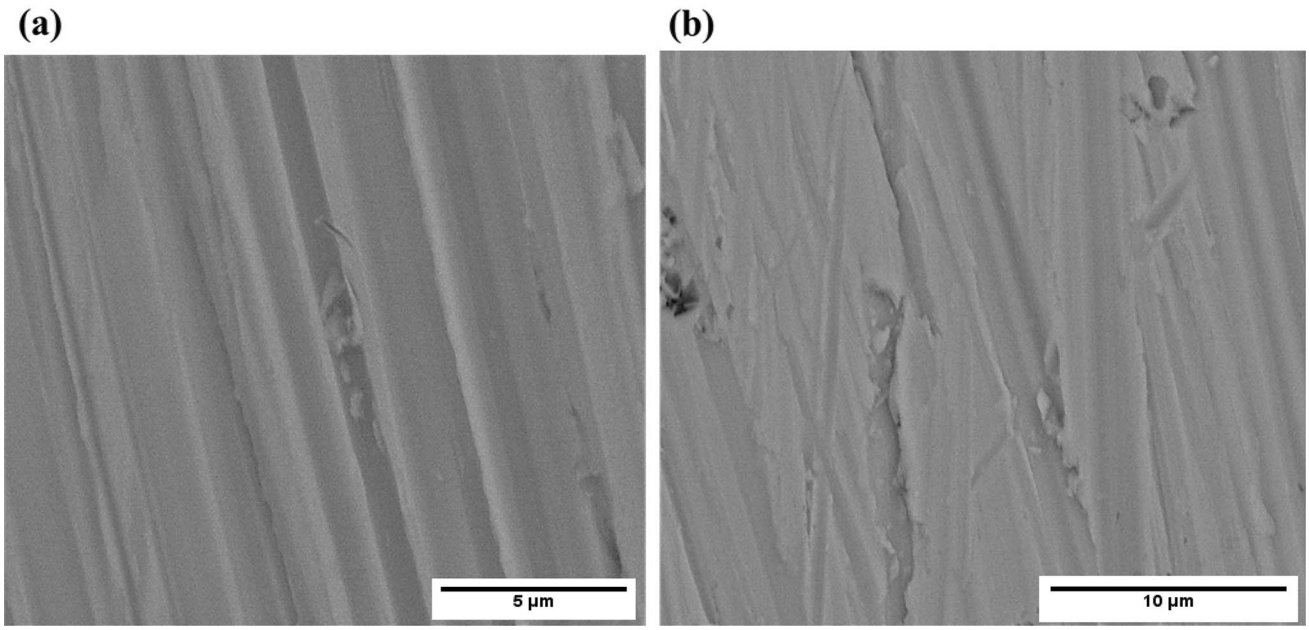

Fig. 2 SEM image of IN738 electrode **a** before and **b** after oxidation

covers the surface. On the other hand, surface deterioration was observed at the edges of the tunnels. Figure 3 represents the EDAX of IN738 surface. The elemental analysis of IN738 surfaces was estimated by EDAX analysis, as reported in Table 1.

According to a previous study of IN738 superalloy microstructure [48, 49], the composite of the alloy consists of a Ni-based austenitic γ matrix, γ' precipitates, and MC carbide in addition to γ/γ' eutectic.

The grain size was expected to be 100 µm. According to the microstructure analysis, two types of carbides were represented in the superalloy located inside the grain boundaries of the γ matrix. The presence of (Ta, Ti) C in addition to a minor percentage of (Nb, W) C was proved by EDAX results.

3.2 Fuel electrooxidation

The electrochemical activity was studied for IN738 electrode toward oxidation of the different small molecules, like ethylene glycol, ethanol, and urea. IN738 is considered a supper alloy with high Ni-contained 50%. Otherwise, the presence of various transition metals in the alloy crystal enhances the catalytic efficacy of the alloy. The activity of the electrode was investigated by cyclic voltammetry (CV) in an alkaline medium of 1.0-M KOH at a scan rate of 20 mV s^{-1}.

Fig. 3 EDAX of IN738 surface

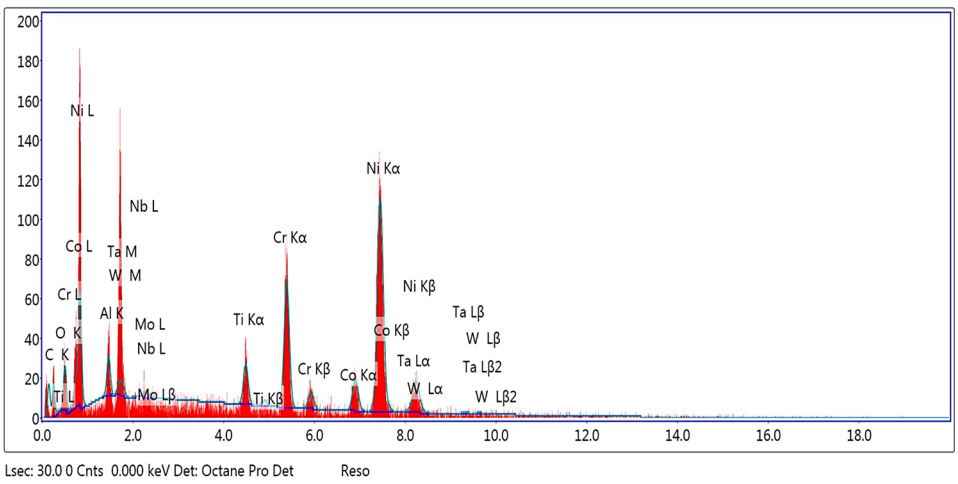

However, the electrooxidation of a small organic molecule on Ni-based catalyst depends on the formation of NiOOH active species followed by electrooxidation of adsorbed fuel molecule as represented in the following Eq. (4) [50]:

$$6Ni(OH)_{2(s)} + 6OH^{-} \rightleftarrows 6NiOOH_{(s)} + 6H_2O_{(l)} + 6e^{-}. \quad (4)$$

The electrode was first activated in KOH to regenerate active species and form metal hydroxides. As shown in Fig. 4a, the electrode was exposed to 50 repeated cycles in a solution of 1.0-M KOH at a scan rate of 100 mV s^{-1}.

Figure 4b shows the CVs of electrochemical oxidation of ethanol, ethylene glycol, and urea upon IN738 surface in a solution of 1.0-M KOH and 1.0 M of fuels at a scan rate of 20 mV s^{-1}. IN738 was the effective surface of the oxidation of these fuels. Consequently, the recognizable oxidation peaks were observed corresponding to the oxidation of each fuel. The higher electrode activity toward ethanol over ethylene glycol is attributed to its simple structure and highest diffusion rate. Additionally, the presence of two hydroxyl groups in ethylene glycol increases the interaction with the solvent and suppresses the molecule's diffusion toward the electrode surface. The adsorption of urea on the metal surface is due to the carbonyl group of urea molecules [51]. Despite the small structure of the urea molecule, it was observed to have the lowest current density owing to the small output electron of complete oxidation compared with ethylene glycol and ethanol counterparts. Furthermore, the direct oxidation of urea leads to the more defined redox peak, as represented in Fig. 4b. The electrochemical oxidation of ethylene glycol is expected to be more complex compared to the urea and ethanol counterparts. The difficulty of complete

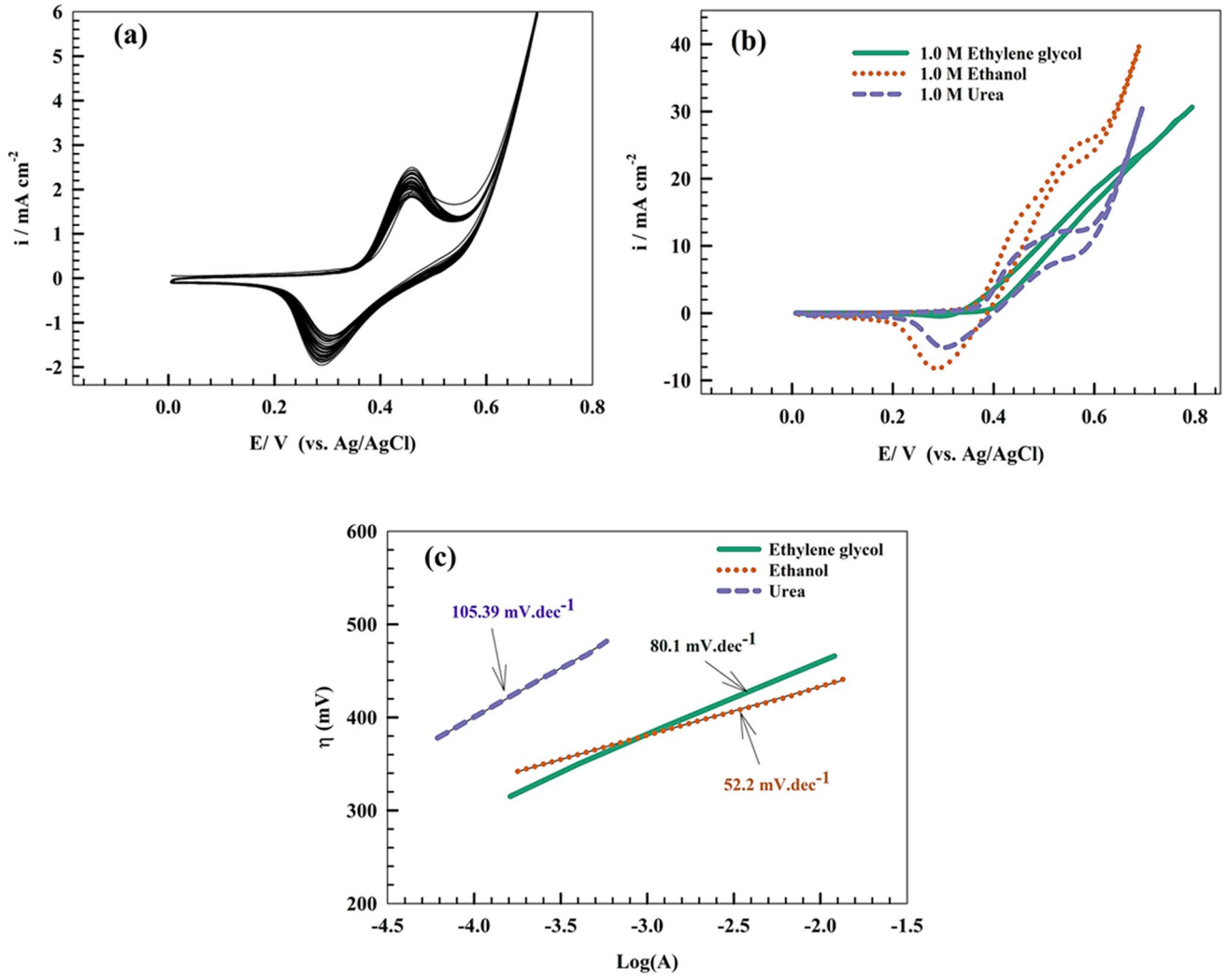

Fig. 4 **a** Repeated 50 CVs at a scan rate of 50 mV s^{-1} for activation of IN738 surface in 1.0 KOH. **b** CVs of IN738-modified electrode at the solution of 1.0 M of (ethylene glycol, ethanol, and urea) in 1.0-M KOH at a scan rate of 20 mV s^{-1}. **c** Tafel plots of (ethylene glycol, ethanol, and urea)

oxidation of ethylene glycol is observed by the undefined oxidation peak and the decrease of the Ni^{2+}/Ni^{3+} peak due to the accumulation of uncomplete oxidative carbon species on the nickel surface.

The activity of different nickel-based surfaces was compared with the result of IN738 for various fuels in an alkaline medium (see Table 2).

Tafel slope is one of the electrochemical parameters obtained from linear sweep voltammetry. The value of Tafel slope reflects how the electrochemical process can take place effectively. Thus, the lower value of Tafel slope indicates the smaller value of potential required to initiate the reaction. As shown in Fig. 4c, Tafel plot of IN738 electrode for ethylene glycol, ethanol, and urea was calculated as 105, 80.2, and 51.2 mV dec^{-1}, respectively. The charge transfer coefficients were also established from Butler–Volmer Eq. (5) [60]:

$$\eta = (2.303\,RT/(1-\alpha)\,\log(i), \tag{5}$$

where η is the over-potential, R is the universal gas constant, T is the operating temperature, n is the number of electrons involved in oxidation ($n_{ethylene\ glycol}=10$, $n_{ethanol}=12$, $n_{urea}=6$), F: is the Faraday constant, and i is the oxidation current.

The charge transfer coefficient (α) was calculated as 0.92, 0.902, and 0.904 for ethylene glycol, ethanol, and urea, respectively. The comparison between electrode activities for different fuels is reported in Table 3.

The concentration of the analyte is considered a vital point for the catalysis process, whereas determining the lower and upper concentration limits can be used to select suitable applications and understand the kinetics of the electrode. Therefore, concentration was studied for different fuels on IN738 electrode. As represented in Fig. 5a–c, the CVs of electrochemical oxidation of ethylene glycol, ethanol, and urea are shown and inset of Fig. 5 shows the linear relation between anodic peak current (at potential of 0.6 V (vs. Ag/AgCl) and fuel concentration (1.0 M). The effect of concentration was studied over concentration ranges (0.025 to 1.0 M). As the result of zero boundary surfaces, the observed anodic current shows two linear regions owing to the electrode's lower sensitivity toward low concentration. Otherwise, the electrode's activity was linear until the concentration reached 1.0 M, indicating a wide range of active species and lower poisoning due to the co-metals inserted in the alloy crystal.

Furthermore, the durability of electrodes was studied using chronoamperometry at oxidation potential (0.55 V vs. Ag/AgCl) for each fuel. The experiment was carried out in a solution of 1.0 M of (ethylene glycol, ethanol, and urea) and 1.0-M KOH for 5 h of continuous oxidation. As shown in Fig. 6a, the chronoamperogram reflects the high stability of IN738 electrode. Consequently, the activity was decreased by a percentage of 9, 7, and 11% for ethylene glycol, ethanol, and urea, respectively. The electrode's durability was expected due to the alloy's CO tolerance as a result of presence of multi-transition metals incorporated in the crystal. Thus, the robust stability of the alloy structure prevents catalyst mass loss.

For constant potential experiments, the current is decreased because of several aspects, like surface poisoning, damage to the electrode surface, and the accumulation of uncompleted

Table 2 The comparison between activities of different catalyst surfaces for ethanol, ethylene glycol, and urea

Surface	Fuel	(OH) Conc (M)	Fuel Conc (M)	Scan rate (mV s^{-1})	Anodic Current (mA cm^{-2})	Ref
Nickel–Copper Multilayer Metal Hydroxide	Ethanol	1.0	0.5	10	26	[52]
nickel nanoparticles	Ethanol	0.5	0.5	5	34	[53]
Ni–Mn double hydroxides	Ethylene glycol	1.0	1.0	20	35	[54]
PdNiP	Ethylene glycol	1.0	1.0	20	31.3	[55]
Sulfonate-MWCNT- PdNi	Ethylene glycol	0.5	1.0	50	35.3	[56]
NiO-Fe_3O_4@Chitosan	Urea	1.0	0.3	10	31	[57]
Cu-doped NiO	Urea	0.5	0.3	20	32	[58]
NiO-MnOx/Polyaniline	Urea	1.0	0.3	50	20	[59]

Table 3 Represent the value of the diffusion coefficient (D), Tafel slope, transfer coefficient (α), onset potentials, and anodic current density (A cm^{-2}) for different fuels electrooxidation upon IN738 anode

Fuel	Tafel slope (mV dec^{-1})	Charge transfer coefficient(α)	Diffusion coefficient ($cm^2\ s^{-1}$) (× 10^{-6})	Onset potential (V)	Anodic peak current (mA cm^{-2})
Ethanol	51.2	0.904	1.5	0.375	29
Ethylene glycol	80.2	0.902	1.038	0.368	17
Urea	105	0.920	0.64	0.391	12

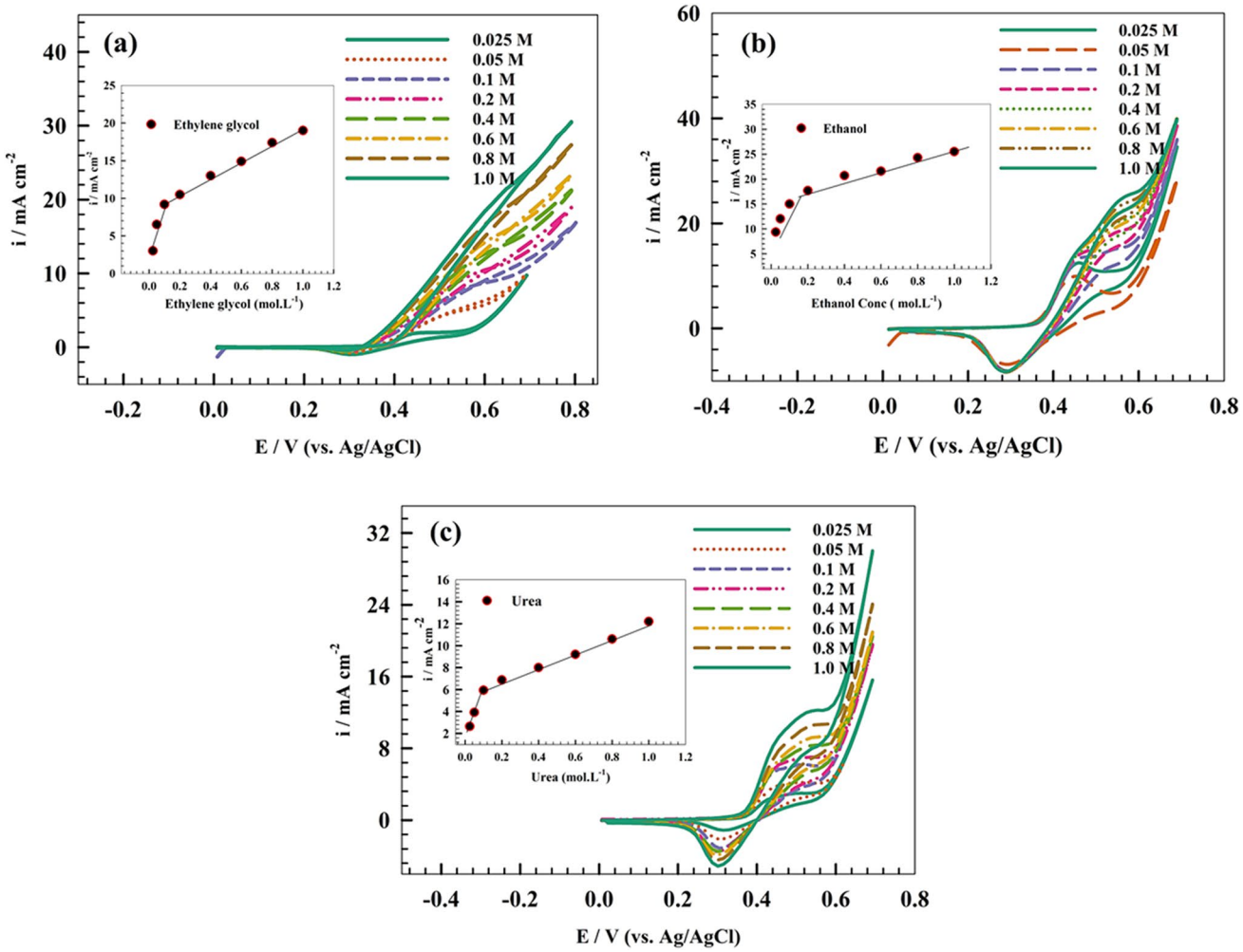

Fig. 5 CVs of IN738 electrode in 1.0-M KOH solution containing different concentrations of **a** ethylene glycol, **b** ethanol, and **c** urea at scan rate 20 mV s^{-1}. Inset Fig. 5: The effect of changing the concentration versus anodic peak current for different fuels

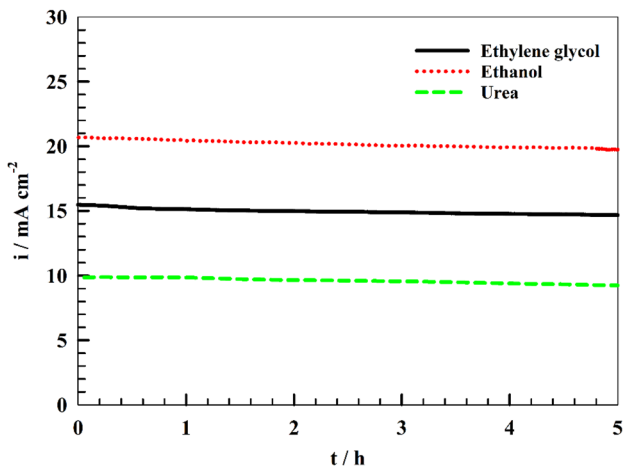

Fig. 6 Representation of long-term electrode stability using chronoamperometry technique for five hours of continuous oxidation

oxidized species [61–63]. Accordingly, the expected CO tolerance of IN738 alloy regards the effect of the co-catalyst, where the Ni-based co-catalyst exhibits high resistance toward CO adsorption [64]. Furthermore, using as-received alloy without casting the catalyst on the electrode surface promotes the surface's stability for long-term oxidation.

3.3 Kinetics study

The electrooxidation in the basic medium is mainly dependent on $Ni(OH)_2$ and NiOOH conversion. Therefore, the estimated surface coverage is calculated by cyclic voltammetry (seen Fig. 7a) in the solution containing 1.0-M KOH for various scan rate ranges as follows (Eq. 6) [65]:

$$J = \left(n^2F^2/4RT\right)\upsilon A\Gamma^{*} \quad (6)$$

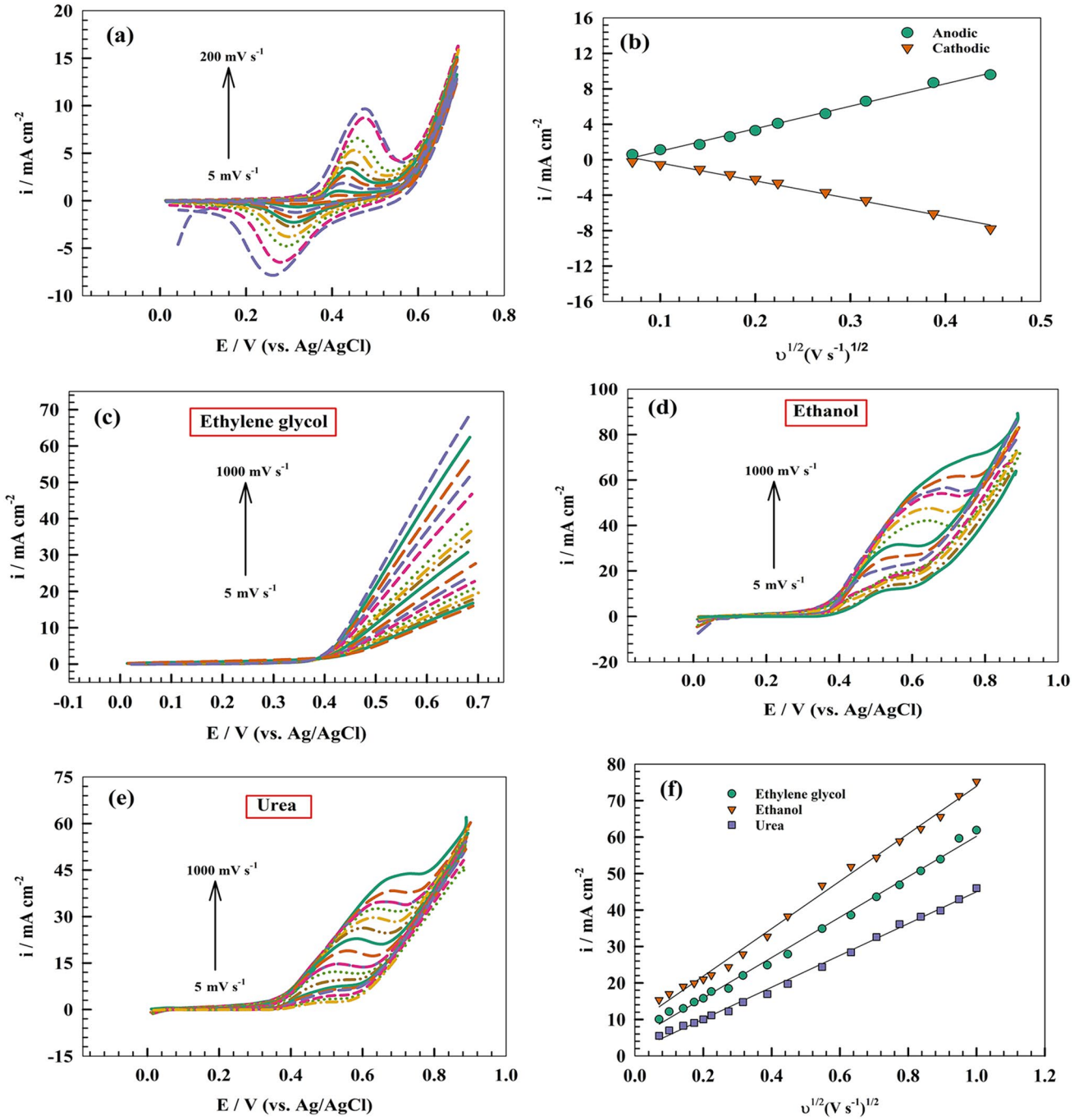

Fig. 7 **a** CVs of IN738 electrode at different scan rates (5–200 mV s^{-1}) in 1.0-M KOH. **b** Anodic and cathodic peak current values of $Ni(OH)_2$/NiOOH redox couple at studied electrocatalysts as a function of the square root of scan rate in the absence of urea. **c-e** Linear sweep voltammetry for different fuels at the 1.0-M KOH and 1.0-M fuel solutions. **f** The relation between I_p of oxidation vs. $\nu^{1/2}$

where J is the oxidation current, n is the electron number, Γ* is the surface coverage, and T is the temperature. Figure 7b displays the linear relation of scan rate vs. oxidation current. That the studied surface coverage equal to 4.199×10^{-7} mol. cm^{-2}, recognization of the electrochemical process and kinetics coefficient must be established. For different fuels,

Fig. 7c–e shows that cyclic voltammetry was employed to find out the diffusion coefficient at a wide sweep rates (5 to 1000 mV s^{-1}). As fuel electrochemical oxidation is considered an irreversible reaction, Randles–Sevcik's relation was used to determine the diffusion coefficient for different fuels toward the IN738 electrode surface. Thus, the diffusion coefficients are provided by the following Eq. (7) [66]:

$$I_p = 2.99 \times 10^5 n(1 - \alpha)\, n_o A C D^{0.5} \upsilon^{0.5}, \quad (7)$$

where I is the current in (A), n is the electron number, n_o is the rate-determining step electron, ν is the scan rate, A is electrode area, C is the fuel concentration, and D is the diffusion coefficient.

Figure 7f shows the relation between the oxidation current (at 0.7 V vs. Ag/AgCl) versus the square root of scan rate along with a wide range of sweep rate, where the diffusion coefficient is provided for ethylene glycol, ethanol, and urea as 1.038×10^{-6}, 1.5×10^{-6}, and 0.64×10^{-6} cm^2 s^{-1}, respectively.

3.4 EIS

For further information about oxidation on IN738 surface, the electrochemical impedance was measured at a constant potential of 0.5 V (vs. Ag/AgCl) in an alkaline solution holding different fuels (i.e., ethylene glycol, ethanol, and urea). Figure 8 displays Nyquist graph for the mentioned fuels. Whereas, the semi-circuit was observed for the charge transfer electrochemical oxidation process.

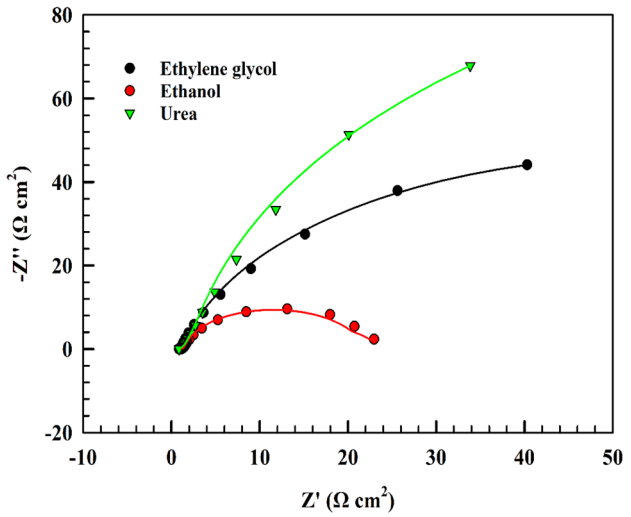

Fig. 8 Nyquist plots of IN738 electrode for electrooxidation of different fuels (ethylene glycol, ethanol, and urea) at the solution of 1.0-M KOH at AC potential 0.55 V

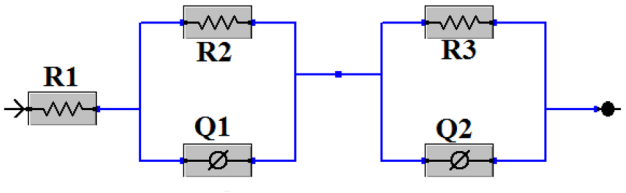

Fig. 9 Fitting circuit of EIS data

The resultant EIS data were fitted by NOVA software, as illustrated in Fig. 9. The solution resistance was connected in series with two cells in the fitting circuit. In each cell, double-layer resistance is connected to a constant phase element in a parallel connection. Accordingly, the presence of the constant phase element was reported in the literature as a surface roughness factor [67]. Otherwise, the constant phase elements are considered for different behaviors, such as distribution of reaction rates, surface thickness, homogeneity, and roughness [67–70].

The estimated EIS parameters are provided in Table 4. It was observed that the impedance of the working electrode in the presence of ethanol is the lowest value among the other fuels. The electrochemical oxidation of ethanol was expected to be easier upon IN738 electrode because of the molecule's lower activation energy and simple structure. The fuel with a higher oxidation current density was found to have lower charge transfer resistance than the other electrodes. Therefore, the faster electron transfer led to higher oxidation activity [71].

4 Conclusion

IN738 superalloy showed efficient electrooxidation of different fuels, like ethylene glycol, ethanol, and urea. The presence of a high percentage of nickel IN738 alloy enhanced the electrochemical activity of IN738 in the alkaline medium. The activity of IN738 toward ethanol is higher than EG fuel due to ethanol's uncomplicated structure and its higher diffusion rate. IN738 has high catalytic efficiency toward urea electrooxidation because of active elements like Co, Cr, Nb, and Mo that boost the performance of the superalloy surface toward urea electrooxidation. The high structural stability of IN738 enhanced the long-term stability of the electrooxidation process and the decrease in current after 4 h of continuous oxidation approached 10% for most cases.

Table 4 The EIS parameters of IN738 electrode in a solution containing 1.0 M of different Fuels (EG, Ethanol, Urea) and 1.0-M KOH at 0.5 V (vs. Ag/AgCl)

Electrode	Element	R_1	R_2	R_3	Q_1		Q_2		
	Parameter	R(Ω cm^{-2})	R(Ω cm^{-2})	R(Ω cm^{-2})	Y_0 (mF)	N	Y_0 (μF)	m	χ^2
Ethanol		0.24	1.54	25	4.38	0.70424	218.12	0.84134	0.04577
Ethylene glycol		0.38	1.66	37.4	5.04	0.6638	292.63	0.82375	0.0739
Urea		0.45	2.02	43.3	5.97	0.63216	314.18	0.85583	0.04604

Author contributions All authors wrote and reviewed the manuscript

Funding Open access funding provided by The Science, Technology & Innovation Funding Authority (STDF) in cooperation with The Egyptian Knowledge Bank (EKB).

Declarations

Conflict of interest The authors declare that there is no conflict of interest regarding the publication of this paper.

References

1. Li Q, Li N, An J, Pang H (2020) Controllable synthesis of a mesoporous NiO/Ni nanorod as an excellent catalyst for urea electro-oxidation. Inorg Chem Front 7:2089–2096
2. Olabi AG, Wilberforce T, Abdelkareem MA (2021) Fuel cell application in the automotive industry and future perspective. Energy 214:118955
3. Li W, Wang D, Zhang Y, Tao L, Wang T, Zou Y, Wang Y, Chen R, Wang S (2020) Defect engineering for fuel-cell electrocatalysts. Adv Mater 32:1907879
4. Borup RL, Kusoglu A, Neyerlin KC, Mukundan R, Ahluwalia RK, Cullen DA, More KL, Weber AZ, Myers DJ (2020) Recent developments in catalyst-related PEM fuel cell durability. Curr Opin Electrochem 21:192–200
5. Abdel Hameed RM, Tammam RH (2018) Nickel oxide nanoparticles grown on mesoporous carbon as an efficient electrocatalyst for urea electro-oxidation. Int J Hydrogen Energy 43:20591–20606. https://doi.org/10.1016/j.ijhydene.2018.09.088
6. Rice C, Ha S, Masel RI, Waszczuk P, Wieckowski A, Barnard T (2002) Direct formic acid fuel cells. J Power Sources 111:83–89
7. El-Khatib KM, Abdel Hameed RM, Amin RS, Fetohi AE (2019) Core-shell structured Pt-transition metals nanoparticles supported on activated carbon for direct methanol fuel cells. Microchem J 145:566–577. https://doi.org/10.1016/j.microc.2018.11.020
8. Abdel Hameed RM, Fahim AE, Allam NK (2020) Tin oxide as a promoter for copper@palladium nanoparticles on graphene sheets during ethanol electro-oxidation in NaOH solution. J Mol Liq 297:111816. https://doi.org/10.1016/j.molliq.2019.111816
9. Maffei N, Pelletier L, Charland JP, McFarlan A (2005) An intermediate temperature direct ammonia fuel cell using a proton conducting electrolyte. J Power Sources 140:264–267
10. Zhang Z, Xin L, Li W (2012) Supported gold nanoparticles as anode catalyst for anion-exchange membrane-direct glycerol fuel cell (AEM-DGFC). Int J Hydrogen Energy 37:9393–9401
11. Ohayre R, Cha SW, Colella W, Prinz FB (2016) Fuel cell fundamentals. John Wiley & Sons, NY
12. Lan R, Tao S, Irvine JTS (2010) A direct urea fuel cell - Power from fertiliser and waste. Energy Environ Sci 3:438–441. https://doi.org/10.1039/b924786f
13. Akhairi MAF, Kamarudin SK (2016) Catalysts in direct ethanol fuel cell (DEFC): An overview. Int J Hydrogen Energy 41:4214–4228
14. Hamnett A (1997) Mechanism and electrocatalysis in the direct methanol fuel cell. Catal Today 38:445–457
15. An L, Zhao TS, Shen SY, Wu QX, Chen R (2010) Performance of a direct ethylene glycol fuel cell with an anion-exchange membrane. Int J Hydrogen Energy 35:4329–4335
16. Livshits V, Philosoph M, Peled E (2008) Direct ethylene glycol fuel-cell stack—Study of oxidation intermediate products. J Power Sources 178:687–691. https://doi.org/10.1016/j.jpowsour.2007.07.054
17. Serov A, Kwak C (2010) Recent achievements in direct ethylene glycol fuel cells (DEGFC). Appl Catal B Environ 97:1–12. https://doi.org/10.1016/j.apcatb.2010.04.011
18. Monyoncho EA, Woo TK, Baranova EA (2018) Ethanol electrooxidation reaction in alkaline media for direct ethanol fuel cells. https://doi.org/10.1039/9781788013895-00001
19. Barakat NAM, Motlak M, Ghouri ZK, Yasin AS, El-Newehy MH, Al-Deyab SS (2016) Nickel nanoparticles-decorated graphene as highly effective and stable electrocatalyst for urea electrooxidation. J Mol Catal A Chem 421:83–91. https://doi.org/10.1016/j.molcata.2016.05.011
20. Atta NF, El-Sherif RMA, Hassan HK, Hefnawy MA, Galal A (2018) Conducting polymer-mixed oxide composite electrocatalyst for enhanced urea oxidation. J Electrochem Soc 165:J3310–J3317. https://doi.org/10.1149/2.0421815jes
21. Hefnawy MA, Medany SS, Fadlallah SA, El-Sherif RM, Hassan SS (2022) Novel Self-assembly Pd(II)-schiff base complex modified glassy carbon electrode for electrochemical detection of paracetamol. Electrocatalysis. https://doi.org/10.1007/s12678-022-00741-7
22. Hefnawy MA, Fadlallah SA, El-Sherif RM, Medany SS (2023) Competition between enzymatic and non-enzymatic electrochemical determination of cholesterol. J Electroanal Chem 930:117169. https://doi.org/10.1016/j.jelechem.2023.117169
23. Zhou Y-W, Chen Y-F, Jiang K, Liu Z, Mao Z-J, Zhang W-Y, Lin W-F, Cai W-B (2021) Probing the enhanced methanol

electrooxidation mechanism on platinum-metal oxide catalyst. Appl Catal B Environ 280:119393
24. Meng X, Ouyang Y, Wu H, Huang H, Wang F, Wang S, Jiang M, Zhang LY (2021) Hierarchical defective palladium-silver alloy nanosheets for ethanol electrooxidation. J Colloid Interface Sci 586:200–207
25. Yang P, Zhou Z, Zheng T, Gu C, Gong X, Zhang Y, Xie Y, Yang N, Fei J (2021) A novel strategy to synthesize Pt/CNTs nanocatalyst with highly improved activity for methanol electrooxidation. J Electroanal Chem 897:115557
26. Yan W, Wang D, Diaz LA, Botte GG (2014) Nickel nanowires as effective catalysts for urea electro-oxidation. Electrochim Acta 134:266–271
27. Guo F, Ye K, Cheng K, Wang G, Cao D (2015) Preparation of nickel nanowire arrays electrode for urea electro-oxidation in alkaline medium. J Power Sources 278:562–568. https://doi.org/10.1016/j.jpowsour.2014.12.125
28. Guo F, Ye K, Du M, Cheng K, Gao Y, Wang G, Cao D (2016) Nickel nanowire arrays electrode as an efficient catalyst for urea peroxide electro-oxidation in alkaline media. Electrochim Acta 190:150–158
29. Wu M-S, Sie Y-J, Yang S-B (2019) Hollow mesoporous nickel dendrites grown on porous nickel foam for electrochemical oxidation of urea. Electrochim Acta 304:131–137
30. Wang G, Ye K, Shao J, Zhang Y, Zhu K, Cheng K, Yan J, Wang G, Cao D (2018) Porous Ni2P nanoflower supported on nickel foam as an efficient three-dimensional electrode for urea electro-oxidation in alkaline medium. Int J Hydrogen Energy 43:9316–9325
31. Ranjani M, Senthilkumar N, Gnana kumar G, Manthiram A (2018) 3D flower-like hierarchical NiCo2O4 architecture on carbon cloth fibers as an anode catalyst for high-performance, durable direct urea fuel cells. J Mater Chem A 6:23019–23027. https://doi.org/10.1039/C8TA08405J
32. Shen F, Jiang W, Qian G, Chen W, Zhang H, Luo L, Yin S (2020) Strongly coupled carbon encapsulated Ni-WO2 hybrids as efficient catalysts for water-to-hydrogen conversion via urea electrooxidation. J Power Sources 458:228014. https://doi.org/10.1016/j.jpowsour.2020.228014
33. Xu W, Du D, Lan R, Humphreys J, Wu Z, Tao S (2017) Highly active Ni–Fe double hydroxides as anode catalysts for electrooxidation of urea. New J Chem 41:4190–4196
34. Forslund RP, Mefford JT, Hardin WG, Alexander CT, Johnston KP, Stevenson KJ (2016) Nanostructured LaNiO3 perovskite electrocatalyst for enhanced urea oxidation. ACS Catal 6:5044–5051
35. Wee S, Do J, Kim K, Lee C, Seok C, Choi B-G, Choi Y, Kim W (2020) Review on mechanical thermal properties of superalloys and thermal barrier coating used in gas turbines. Appl Sci 10:5476
36. Wan Z, Wang T, Sun Y, Hu L, Li Z, Li P, Zhang Y (2018) Dynamic softening mechanisms of GH4720Li alloyduring hot deformation. Acta Met Sin 55:213–222
37. Peters M, Kumpfert J, Ward CH, Leyens C (2003) Titanium alloys for aerospace applications. Adv Eng Mater 5:419–427
38. Perrut M, Caron P, Thomas M, Couret A (2018) High temperature materials for aerospace applications: Ni-based superalloys and γ-TiAl alloys. Comptes Rendus Phys 19:657–671
39. Singh K (2014) Advanced materials for land based gas turbines. Trans Indian Inst Met 67:601–615
40. Grange D, Queva A, Guillemot G, Bellet M, Bartout J-D, Colin C (2021) Effect of processing parameters during the laser beam melting of Inconel 738: comparison between simulated and experimental melt pool shape. J Mater Process Technol 289:116897
41. Hassan HB, Hamid ZA (2011) Electrodeposited Ni–Cr2O3 nanocomposite anodes for ethanol electrooxidation. Int J Hydrogen Energy 36:5117–5127
42. Yan X, Zhang W-D, Xu H, Xiang L, Liu J, Yang J, Zhu H, Gu Z-G (2021) Hierarchical NiCr hydroxide nanospheres with tunable domain boundaries for highly efficient urea electro-oxidation. Electrochim Acta 388:138633
43. Ruiz-López E, Diaz-Perez MA, de Lucas-Consuegra A, Dorado F, Serrano-Ruiz JC (2021) Membrane-less ethanol electrooxidation over Pd-M (M: Sn, Mo and Re) bimetallic catalysts. Catalysts 11:541
44. Chaitree W, Kalu EE, Liang Z, Yeboah YD (2021) Effects of bath composition and thermal treatment on the performance of Co-Ni-Mo-P electrocatalyst supported on carbon for the electro-oxidation of ethanol. J Alloys Compd 860:158404
45. Qi L, Guo X, Zheng X, Wang Y, Zhao Y, Wang X (2021) Enhanced electrocatalytic activity of urchin-like Nb2O5 microspheres by synergistic effects with Pd toward electrooxidation of ethylene glycol in an alkaline medium. Mol Catal 504:111436
46. Ling L-S-B, Yin Z, Hu Z, Liang J-H, Wang Z-Y, Wang J, Sun B-D (2019) Effects of the γ″-Ni3Nb phase on mechanical properties of inconel 718 superalloys with different heat treatments. Materials (Basel) 13:151. https://doi.org/10.3390/ma13010151
47. Mrozowski N, Hénaff G, Hamon F, Rouffié A-L, Franchet J-M, Cormier J, Villechaise P (2020) Aging of γ′ Precipitates at 750 °C in the nickel-based superalloy AD730TM: A thermally or thermo-mechanically controlled process? Metals. https://doi.org/10.3390/met10040426
48. El-Bagoury N, Waly M, Nofal A (2008) Effect of various heat treatment conditions on microstructure of cast polycrystalline IN738LC alloy. Mater Sci Eng A 487:152–161. https://doi.org/10.1016/j.msea.2007.10.004
49. El-Bagoury N, Nofal A (2010) Microstructure of an experimental Ni base superalloy under various casting conditions. Mater Sci Eng A 527:7793–7800. https://doi.org/10.1016/j.msea.2010.08.050
50. Galal A, Atta NF, Hefnawy MA (2020) Lanthanum nickel oxide nano-perovskite decorated carbon nanotubes/poly (aniline) composite for effective electrochemical oxidation of urea. J Electroanal Chem 862:114009
51. Abidin MNZ, Goh PS, Ismail AF, Said N, Othman MHD, Hasbullah H, Abdullah MS, Ng BC, Kadir SHSA, Kamal F (2018) Highly adsorptive oxidized starch nanoparticles for efficient urea removal. Carbohydr Polym 201:257–263. https://doi.org/10.1016/j.carbpol.2018.08.069
52. A.A. Maizelis, Electrooxidation of ethanol on nickel-copper multilayer metal hydroxide electrode, in: Int. Conf. Nanotechnol. Nanomater., Springer, 2018: pp. 59–68.
53. Vyas AN, Desai MA, Phase DM, Saratale RG, Ambekar JD, Kale BB, Pathan HM, Sartale SD (2019) Nickel nanoparticles grown by successive ionic layer adsorption and reaction method for ethanol electrooxidation and electrochemical quartz crystal microbalance study. New J Chem 43:2955–2965. https://doi.org/10.1039/C8NJ04984J
54. Hefnawy MA, Fadlallah SA, El-Sherif RM, Medany SS (2021) Nickel-manganese double hydroxide mixed with reduced graphene oxide electrocatalyst for efficient ethylene glycol electrooxidation and hydrogen evolution reaction. Synth Met 282:116959. https://doi.org/10.1016/j.synthmet.2021.116959
55. Yu Z, Xu J, Amorim I, Li Y, Liu L (2021) Easy preparation of multifunctional ternary PdNiP/C catalysts toward enhanced small organic molecule electro-oxidation and hydrogen evolution reactions. J Energy Chem 58:256–263. https://doi.org/10.1016/j.jechem.2020.10.016
56. Ramulifho T, Ozoemena KI, Modibedi RM, Jafta CJ, Mathe MK (2013) Electrocatalytic oxidation of ethylene glycol at palladium-bimetallic nanocatalysts (PdSn and PdNi) supported on

sulfonate-functionalised multi-walled carbon nanotubes. J Electroanal Chem 692:26–30. https://doi.org/10.1016/j.jelechem.2012.12.010
57. Hefnawy MA, Medany SS, El-Sherif RM, Fadlallah SA (2022) Green synthesis of NiO/Fe3O4@chitosan composite catalyst based on graphite for urea electro-oxidation. Mater Chem Phys 290:126603. https://doi.org/10.1016/j.matchemphys.2022.126603
58. Hefnawy MA, Fadlallah SA, El-Sherif RM, Medany SS (2021) Synergistic effect of Cu-doped NiO for enhancing urea electrooxidation: comparative electrochemical and DFT studies. J Alloys Compd. https://doi.org/10.1016/j.jallcom.2021.162857
59. Hefnawy MA, Medany SS, El-Sherif RM, Fadlallah SA (2022) NiO-MnOx/Polyaniline/Graphite Electrodes for Urea Electrocatalysis: Synergetic Effect between Polymorphs of MnOx and NiO. ChemistrySelect 7:e202103735. https://doi.org/10.1002/slct.202103735
60. Galal A, Atta NF, Hefnawy MA (2020) Voltammetry study of electrocatalytic activity of lanthanum nickel perovskite nanoclusters-based composite catalyst for effective oxidation of urea in alkaline medium. Synth Met 266:116372. https://doi.org/10.1016/j.synthmet.2020.116372
61. Wu F, Eid K, Abdullah AM, Niu W, Wang C, Lan Y, Elzatahry AA, Xu G (2020) Unveiling one-pot template-free fabrication of exquisite multidimensional PtNi multicube nanoarchitectonics for the efficient electrochemical oxidation of ethanol and methanol with a great tolerance for CO. ACS Appl Mater Interfaces 12:31309–31318
62. Forslund RP, Mefford JT, Hardin WG, Alexander CT, Johnston KP, Stevenson KJ (2016) Nanostructured LaNiO3Perovskite electrocatalyst for enhanced urea oxidation. ACS Catal 6:5044–5051. https://doi.org/10.1021/acscatal.6b00487
63. Basumatary P, Lee UH, Konwar D, Yoon YS (2020) An efficient tri-metallic anodic electrocatalyst for urea electro-oxidation. Int J Hydrogen Energy 45:32770–32779
64. Hefnawy MA, Fadlallah SA, El-Sherif RM, Medany SS (2023) Systematic DFT studies of CO-Tolerance and CO oxidation on Cu-doped Ni surfaces. J Mol Graph Model 118:108343. https://doi.org/10.1016/j.jmgm.2022.108343
65. Abdel Hameed RM, Medany SS (2017) Enhanced electrocatalytic activity of NiO nanoparticles supported on graphite planes towards urea electro-oxidation in NaOH solution. Int J Hydrogen Energy 42:24117–24130. https://doi.org/10.1016/j.ijhydene.2017.07.236
66. Hameed RMA, Medany SS (2019) Improved electrocatalytic kinetics of nickel hydroxide nanoparticles on Vulcan XC-72R carbon black towards alkaline urea oxidation reaction. Int J Hydrogen Energy 44:3636–3648
67. Maritan A, Toigo F (1990) On skewed ARC plots of impedance of electrodes with an irreversible electrode process. Electrochim Acta 35:141–145
68. Barsoukov E, Macdonald JR (2005) Impedance Spectroscopy Theory, Experiment and Appl, 2nd edn. John Wiley & Sons, Hoboken
69. Schiller CA, Strunz W (2001) The evaluation of experimental dielectric data of barrier coatings by means of different models. Electrochim Acta 46:3619–3625
70. Kim C-H, Pyun S-I, Kim J-H (2003) An investigation of the capacitance dispersion on the fractal carbon electrode with edge and basal orientations. Electrochim Acta 48:3455–3463
71. Döner A, Telli E, Kardaş G (2012) Electrocatalysis of Ni-promoted Cd coated graphite toward methanol oxidation in alkaline medium. J Power Sourc 205:71–79

Authors and Affiliations

Mahmoud A. Hefnawy[1] · Shymaa S. Medany[1] · Rabab M. El-Sherif[1] · Nader El-Bagoury[2] · Sahar A. Fadlallah[1]

✉ Sahar A. Fadlallah
sahmed@sci.cu.edu.eg; sahar.fadlallah@yahoo.com

[1] Chemistry Department, Faculty of Science, Cairo University, Giza 12613, Egypt

[2] Central Metallurgical Research and Development Institute, CMRDI, Helwan, Cairo, Egypt